RAA 2015 Vol. **15** No. **5**, 663–672 doi: 10.1088/1674–4527/15/5/005
http://www.raa-journal.org *http://www.iop.org/journals/raa*

Research in Astronomy and Astrophysics

The relationship between the properties of PAHs and AGN activities in type-I AGNs *

Qi-Chen Feng[1,2], Jing Wang[1,3], Hua-Li Li[1,2] and Jian-Yan Wei[1,3]

[1] National Astronomical Observatories, Chinese Academy of Sciences, Beijing 100012, China; *fqch@bao.ac.cn*
[2] University of Chinese Academy of Sciences, Beijing 100049, China
[3] Key Laboratory of Space Astronomy and Technology (NAOC, CAS), Beijing 100012, China

Received 2014 May 8; accepted 2014 August 12

Abstract In order to explore the relationship between properties of Polycyclic Aromatic Hydrocarbons (PAHs) and AGN activities in Type-I AGNs, we compiled a sample of 47 Type-I AGNs with measured PAH 11.3 μm and 7.7 μm emission lines. The PAH emission and optical properties of these AGNs are taken from the literature. It is found that the equivalent width (EW) of 11.3 μm emission from PAHs shows a weak correlation with the ratio of the EWs of the FeII complex between λ4434 and λ4684 to Hβ (RFe). The PAH 11.3/7.7 ratio is correlated with various elements defined by the first eigenvector space, which are RFe, [OIII]λ5007 luminosity and Hβ asymmetry. These correlations infer that AGNs with high RFe, weak [OIII] emission and a strong Hβ blue-wing are likely to have low PAH ionization, and hence a larger amount of neutral PAHs.

Key words: infrared: ISM — quasars: emission lines — galaxies: active — galaxies: evolution — methods: statistical

1 INTRODUCTION

A Polycyclic Aromatic Hydrocarbon (PAH) is a kind of aromatic molecule which is made up of 10∼1000 carbon atoms. The diameter of a PAH is usually several Å (Leger & Puget 1984; Allamandola et al. 1985). PAHs exist everywhere and are especially located in the interstellar medium (ISM), and most nearby galaxies with ongoing or recent star-formation regions. This phenomenon has been widely observed recently by the highly sensitive *Spitzer Space Telescope* (Peeters et al. 2004; Smith et al. 2007b; Galliano et al. 2008) and *Infrared Space Observatory* (*ISO*; Genzel & Cesarsky 2000). A PAH can be excited by the absorption of ultraviolet photons, and then it re-emits the incident energy into the infrared (IR) band through vibrational modes of the carbon skeleton. Many *Spitzer* spectra of nearby Seyfert galaxies show strong contributions from star-forming features in the form of PAH bands (Clavel et al. 2000; Buchanan et al. 2006; Tommasin et al. 2008).

There are several prominent PAH emission lines in the mid-infrared at 3.3, 6.2, 7.7, 11.3 and 17 μm, in the zone from 3 to 19 μm. Since each feature is attributed to a given vibrational mode, the

* Supported by the National Natural Science Foundation of China.

ratio between these features will vary with quantities such as the charge, the hydrogenation, or the size and shape of the molecule (Galliano et al. 2008). The 11.3 μm feature is thought to be produced by neutral PAHs, whereas the 7.7 μm feature arises primarily from PAH cations (Allamandola et al. 1999; Draine & Li 2001). PAH grains can be modeled as spanning a range in size from very small amorphous carbon dust to very large carbon-rich ring molecules (Puget & Leger 1989; Draine & Lee 1984; Draine & Li 2001).

The equivalent width (EW) of PAH emission from a given galaxy can be used as a diagnostic to probe the relative amount of star-formation to AGN activity. Previous studies have suggested that PAH EWs are anti-correlated with the presence of increasing AGN activity. LaMassa et al. (2012) argued the reasons for this phenomenon are that either the mid-IR continuum rises to bury the PAH EW, or the hard ionization field destroys the PAH grain. They also compared the correlations between [Ne V]/[Ne II] and various PAH ratios, such as 7.7/17, 11.3/17 and 11.3/7.7, and found that the 11.3 μm feature could be strongly suppressed in most AGN-dominated systems.

In Type-I AGNs, Boroson & Green (1992, BG92) found that there are strong correlations among RFe, [OIII]λ5007 luminosity, Hβ full width at half maximum (FWHM) and Hβ asymmetry, a collection which is called Eigenvector 1 (E1). E1 has been extended since then to include soft X-ray index $\Gamma_{\rm soft}$ (Wang et al. 1996; Sulentic et al. 2000, 2002, 2004; Xu et al. 2003; Grupe et al. 1999; Grupe 2004; Laor et al. 1997; Lawrence et al. 1997; Vaughan et al. 2001), infrared color α (60,25), flux ratio [OIII]/Hβ_n (Wang et al. 2006), and optical variability amplitude (Mao et al. 2009). E1 plays a very important role in understanding the basic properties of AGNs. Boroson (2002) indicated that values associated with E1 are dominated by the Eddington ratio.

In this paper, we try to investigate the correlations between PAH emission lines and E1. The sample selection is shown in Section 2; we give the results in Section 3 and a simple physical discussion of the identified correlations related with PAH line ratios is provided in Section 4. The last section is a short conclusion drawn from the results.

2 SAMPLE

Our selected sample has 47 Type I AGNs in total which are selected from three different papers. The main part of the sample, 40 Palomar-Green (PG) quasars and two Third Cambridge Catalogue (3C) radio galaxies with redshift $z < 0.5$, is from Shi et al. (2007). Two AGNs, 3C 120 and NGC 6251, are selected from Ogle et al. (2010). NGC 3227, NGC 4051 and NGC 7469 are from Diamond-Stanic & Rieke (2010). The PAH 11.3 μm and 7.7 μm fluxes, and their EWs, are listed in Table 1.

Shi et al. (2007) used the *Spitzer* standard staring mode to observe the targets. The intermediate products of the *Spitzer* Science Center (SSC) pipeline versions S13.0.1, S13.2.0 and S15.3.0 were processed within the SMART software package (Higdon et al. 2004). They used the Short-Low (SL) module 3.6″ slit and the Long-Low (LL) module 10.5″ slit. The shapes of the PAH features are assumed to be Drude profiles. The 7.7 μm PAH feature is located at the blue end of the silicate feature. To remove this effect, they fit the blue wing of the silicate feature with a Doppler profile. The continuum underlying the 7.7 μm PAH features is defined as power laws over three narrow regions (5.2–5.5, 5.5–5.8 and 6.7–7.0 μm) that are free from line or feature emission. They fit the continua-subtracted spectra simultaneously with PAH 7.7 μm. For the 11.3 μm feature, the continuum shape is defined by using a quadratic interpolation over the four continuum spectral regions, 9.7–10.0, 10.0–10.3, 10.7–11.0 and 11.7–12.1 μm (Shi et al. 2007).

Ogle et al. (2010) used pipeline versions S15–S17 and basic calibrated data (BCDs) sets. They used the slits of the SL and LL modules and the Drude profile to measure both PAH 7.7 μm and 11.3 μm features, with the software PAHFIT written by Smith et al. (2007b). The relatively smaller uncertainties are listed in Table 1.

Diamond-Stanic & Rieke (2010) gathered data from the *Spitzer* archive taken with the Infrared Spectrograph (IRS) SL module. They used CUBISM (Smith et al. 2007a) to extract one-dimensional

spectra from BCD taken with the 3.6″ slit. They also used the Drude profile to measure both PAH 7.7 μm and 11.3 μm features with the software PAHFIT. The relatively smaller uncertainties are also listed in Table 1.

The optical data of the sample (RFe, Hβ asymmetry and [OIII] luminosity) are extracted from published literature and listed in Table 1. RFe and Hβ asymmetry are mainly from BG92. RFe is the ratio of the equivalent widths of the FeII complex between λ4434 and λ4684 to Hβ. Hβ asymmetry, defined by De Robertis (1985), is the measurement of the shift between the centroids at 1/4 and 3/4 maximum in units of FWHM. A positive value of Hβ asymmetry means that the profile has a blue wing. The logarithm values of [OIII]λ5007 luminosities and the details of the references are listed in Table 1.

Comparing these three papers, we noticed that they used two kinds of methods to fit the PAH features with Drude profiles. Both Ogle et al. (2010) and Diamond-Stanic & Rieke (2010) used PAHFIT, in which PAH features are recovered from full feature decomposition. Shi et al. (2007) used a method in which PAH features are measured under the assumption that the underlying continuum could be obtained from power-law or spline fits. Smith et al. (2007b) pointed out that PAH 11.3 μm emission measured from these two methods could be different by a ratio of about 1.75, and PAH 7.7 μm emission by a ratio even above 3. The spline method generally underestimates the feature strengths of the PAHs. The systematic differences in methods may affect the results of correlation analyses. However, because only five AGNs are measured with the PAHFIT method, this has only a small effect on the final results of the total sample. We will check this in more detail in Section 4.

3 RESULTS

RFe is a key element of E1. Thus, we first explore the relationship between RFe and the PAH emission lines. In Figure 1, we plot the logarithm of PAH 11.3 μm EWs versus RFe in a sub-sample of 40 Type-I AGNs. A Spearman Rank-Order test is performed and returns $\rho = 0.313$ and $p = 0.0506$. The parameter ρ is the correlation coefficient; the parameter p is the probability that a correlation is not present. There is a tendency in which RFe increases with the PAH 11.3 μm EW.

In Figure 2, the logarithm of PAH 7.7 μm EWs versus RFe is plotted for a sub-sample of 26 AGNs. The Kendall Rank-Order test returns a result of $\tau = 0.1846$ and $p = 0.1836$. The parameter τ is similar to ρ, evaluating the strength of the correlation between two variables. Thus, there is no obvious correlation between RFe and the PAH 7.7 μm EW. We use the Kendall Rank-Order test here, since it is especially suitable for a small sample. The Spearman Rank-Order test is better for samples with more than 30 members.

In Figure 3, we plot the PAH 11.3 μm/PAH 7.7 μm ratio versus RFe in a sub-sample of 31 AGNs. The Spearman Rank-Order test returns a correlation coefficient of $\rho = 0.618$ at a significance level of $p = 0.0007$. Therefore, there is a correlation between the PAH 11.3 μm/7.7 μm ratio and RFe.

We next search for the relationship between the PAH 11.3/7.7 ratio and other elements of E1. In Figure 4, the PAH 11.3/7.7 ratio versus [OIII]λ5007 luminosity is plotted in a sub-sample of 27 AGNs. The Kendall Rank-Order test returns $\tau = -0.4473$ and $p = 0.0011$. Thus, there is a relatively strong anti-correlation between optical [OIII] luminosity and the PAH 11.3/7.7 ratio.

In Figure 5, we plot the PAH 11.3 μm/7.7 μm versus Hβ asymmetry in a sub-sample of 26 AGNs. The Kendall Rank-Order test returns $\tau = 0.3662$ and $p = 0.0087$. There is a correlation between Hβ asymmetry and the PAH 11.3/7.7 ratio.

The above results indicate that the PAH 11.3/7.7 ratio has an obvious correlation with the primary elements of E1. Like BG92, we calculated the complete correlation matrix for a set of parameters and generated eigenvectors associated with the correlation matrix. All the correlation coefficients listed in Table 2 are calculated by the Kendall Rank-Order test. The PAH 7.7 μm and 11.3 μm luminosities in Table 2 were calculated by

$$L = 4\pi D_{\rm L}^2 F_{\rm PAH}\,, \tag{1}$$

Table 1 Properties of PAHs, RFe, [OIII] luminosity and Hβ asymmetry in the sample of Type-I AGNs.

Name	z	PAH EW 7.7 μm	PAH EW 11.3 μm	PAH flux 7.7 μm	PAH flux 11.3 μm	PAH 11.3 μm/7.7 μm	RFe	[OIII] luminosity	Hβ asymmetry
(1)	(2)	(3)	(4)	(5)	(6)	(7)	(8)	(9)	(10)
PG 0003+199	0.025		0.01		0.29±0.06		0.62		
PG 0007+106	0.089		0.03		0.51±0.06		0.35		
PG 0050+124	0.061	0.05	0.02	8.28±5.61	2.77±0.25	0.335±0.229	1.47	41.87	0.09
PG 0052+251	0.155		0.05		0.55±0.12		0.23		
PG 0157+001	0.163	0.25	0.09	6.71±2.44	2.44±0.16	0.364±0.134	1.36	40.87	0.003
PG 0844+349	0.064	0.09	0.03	1.56±0.60	0.38±0.07	0.244±0.104	0.89	41.99	0.059
PG 0923+129	0.029	0.28	0.08	9.73±2.28	2.42±0.13	0.249±0.060	0.53	41.65	−0.031
PG 0934+013	0.05	0.26	0.08	2.86±0.60	0.74±0.05	0.259±0.057	0.48		−0.084
PG 1001+054	0.16		0.03		0.17±0.03		0.82		
PG 1004+130	0.24		0.02		0.20±0.05		0.23		
PG 1011–040	0.058		0.03		0.50±0.04		0.73		
PG 1022+519	0.044	0.44	0.19	4.22±0.74	1.32±0.08	0.313±0.058	1.08	41.26	0.038
PG 1049–005	0.359	0.07	0.01	1.17±0.38	0.17±0.07	0.145±0.076	0.56	43.28	−0.044
PG 1100+772	0.311		0.04		0.29±0.08		0.21		
PG 1115+407	0.154	0.28	0.08	2.55±0.33	0.46±0.03	0.180±0.026	0.54		−0.025
PG 1119+120	0.05	0.06	0.03	2.26±0.89	0.80±0.09	0.354±0.145	0.9	41.67	−0.01
PG 1126–041	0.06		0.04		1.35±0.36		1.07		
PG 1202+281	0.165	0.14	0.04	1.41±0.48	0.37±0.05	0.262±0.096	0.29	42.49	−0.298
PG 1229+204	0.063		0.02		0.38±0.12		0.59		
PG 1244+026	0.048	0.14	0.04	1.76±0.86	0.51±0.04	0.290±0.143	1.2	41.47	0.112
PG 1310–108	0.034	0.11	0.01	2.40±0.86	0.18±0.03	0.075±0.030	0.38	41.89	−0.075
PG 1322+659	0.168	0.07	0.03	0.72±0.30	0.20±0.02	0.278±0.119	0.59	42.22	−0.009
PG 1341+258	0.087	0.06	0.02	0.45±0.21	0.11±0.02	0.244±0.122	0.38		−0.066
PG 1351+236	0.055	0.87	0.44	7.54±1.05	2.75±0.12	0.365±0.053	1.18	41.39	0.135
PG 1404+226	0.098	0.14	0.05	0.88±0.37	0.25±0.02	0.284±0.122	1.01	41.61	0.112
PG 1411+442	0.089		0.01		0.31±0.04		0.49		
PG 1415+451	0.113	0.14	0.1	1.67±0.30	0.86±0.06	0.515±0.099	1.6	41.03	0.106
PG 1426+015	0.086	0.03	0.01	1.19±0.64	0.31±0.06	0.261±0.149	0.39	41.47	0.033
PG 1440+356	0.079	0.2	0.1	6.74±2.89	2.27±0.13	0.337±0.146	1.19	42.1	−0.026
PG 1448+273	0.065	0.11	0.07	1.98±0.59	0.94±0.06	0.475±0.145	0.9		0.041
PG 1519+226	0.137	0.04	0.02	0.59±0.21	0.21±0.02	0.356±0.131	1.01	41.61	0.095
PG 1534+580	0.029	0.05	0.02	1.45±0.72	0.44±0.08	0.303±0.16	0.27	41.51	0.044
PG 1535+547	0.038	0.02	0.01	0.62±0.22	0.08±0.03	0.129±0.067	0.47	41.54	0.021
PG 1552+085	0.119		0.02		0.11±0.02		1.02		
PG 1612+261	0.13		0.03		0.38±0.22		0.18		
PG 1613+658	0.129	0.08	0.03	3.02±1.87	0.77±0.09	0.255±0.161	0.38	42.89	−0.207
PG 2112+059	0.466		0.02		0.27±0.05		0.63		
PG 2130+099	0.062	0.06	0.01	4.20±1.29	0.55±0.21	0.131±0.064	0.64	42.65	−0.109
PG 2209+184	0.07	0.2	0.06	1.32±0.37	0.29±0.03	0.220±0.066	0.44	42.18	0.051
PG 2349–014	0.174		0.05		0.41±0.10				
3C 249.1	0.311		0.04		0.29±0.10		0.54		
3C 293	0.045	0.62	0.41	3.96±0.70	1.27±0.10	0.321±0.062			
3C 120	0.033			11.7±1.4	3.3±0.2	0.282±0.038	0.24	41.8	
NGC 3227	0.004			9.99±0.15	3.24±0.03	0.324±0.005	0.54	41.23	
NGC 4051	0.002			4.42±0.31	1.12±0.03	0.253±0.019	1.1	41.31	
NGC 7469	0.016			29.3±0.6	5.41±0.05	0.185±0.004	0.27	41.84	
NGC 6251	0.025			0.66±0.1	0.27±0.02	0.409±0.069	1.67	39.78	

Notes: Cols. (3)–(4): PAH EW 7.7 and 11.3 μm in units of microns. Cols.(5)–(6): PAH flux 7.7 and 11.3 μm in units of 10^{-13} erg s^{-1} cm^{-2}. Col.(9): logarithm of [OIII] luminosity. References: Cols. (3)–(4) Shi et al. (2007); Cols. (5)–(7) Shi et al. (2007); Diamond-Stanic & Rieke (2010); Ogle et al. (2010); Col. (8) Boroson & Green (1992); Kuraszkiewicz et al. (2000); Wang et al. (2006); Grupe et al. (2004); Col. (9) Meléndez et al. (2008); Laor et al. (1997); Bonatto & Pastoriza (1997); Brightman & Nandra (2011); Kraemer et al. (2004); Stockton & MacKenty (1987); Whittle (1992); Alonso-Herrero et al. (1997); Zhang & Wang (2006); van der Wolk et al. (2010); Kuraszkiewicz et al. (2000); Maiolino et al. (2007); Col. (10) Boroson & Green (1992).

Table 2 Correlation Coefficient Matrix

Name	PAH EW 7.7 μm	PAH EW 11.3 μm	L (PAH 7.7 μm)	L (PAH 11.3 μm)	PAH 11.3/7.7	RFe	L [OIII]	Hβ asymmetry	$\log R$
(1)	(2)	(3)	(4)	(5)	(6)	(7)	(8)	(9)	(10)
PAH 7.7 μm EW		0.6923	0.1508	0.2037	0.12435	0.1846	−0.06495	0.01975	0.13665
PAH 11.3 μm EW	0.6923		0.18235	0.26175	0.3419	0.28615	−0.16885	0.1186	0.10335
L(PAH 7.7 μm)	0.1508	0.18235		0.7839	0.09885	0.08375	0.22335	−0.0684	0.04335
L(PAH 11.3 μm)	0.2037	0.26175	0.7839		0.25055	0.0134	0.07	0.0285	0.10335
PAH 11.3/7.7	0.12435	0.3419	0.09885	0.25055		0.33065	−0.4524	0.40615	0.17665
RFe	0.1846	0.28615	0.08375	0.0134	0.33065		−0.2381	0.32195	0
L[OIII]	−0.06495	−0.16885	0.22335	0.07	−0.4524	−0.2381		−0.5257	−0.20475
Hβ asymm	0.01975	0.1186	−0.0684	0.0285	0.40615	0.32195	−0.5257		0.18665
$\log R$	0.13665	0.10335	0.04335	0.10335	0.17665	0	−0.20475	0.18665	

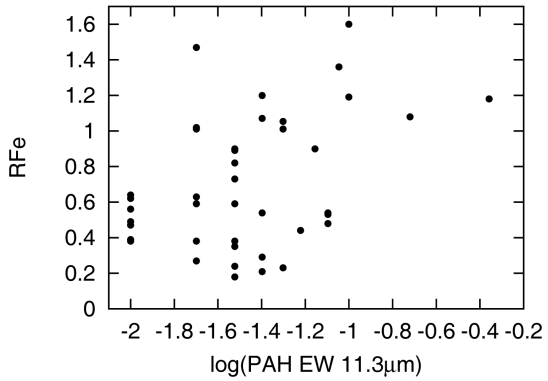

Fig. 1 PAH 11.3 EW vs. RFe: the PAH 11.3 μm EWs are correlated with RFe and the correlation coefficient is $\rho = 0.314$. It shows a weak correlation here.

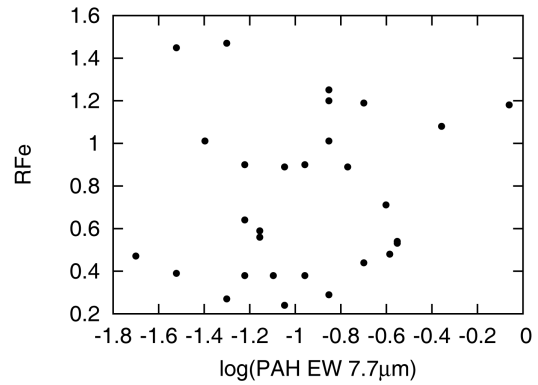

Fig. 2 PAH 7.7 EW vs. RFe: the PAH 7.7 μm EWs are not correlated with RFe. The calculated correlation coefficient is $\tau = 0.0739$.

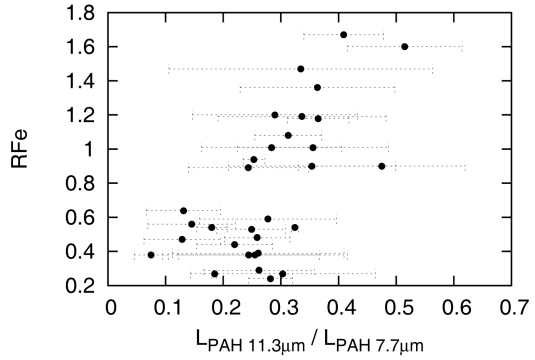

Fig. 3 PAH 11.3 μm/PAH 7.7 μm vs. RFe: it shows a correlation between the PAH 11.3/7.7 ratio and RFe. The correlation coefficient is $\rho = 0.469$.

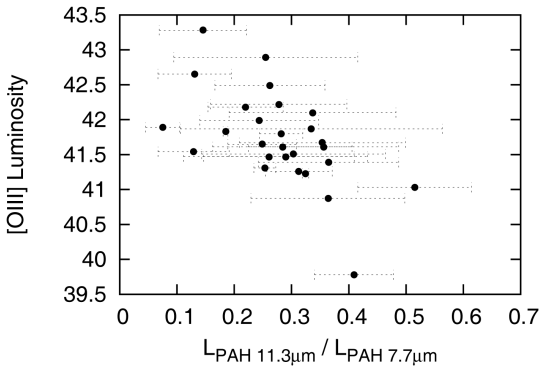

Fig. 4 PAH 11.3 μm/PAH 7.7 μm vs. [OIII] luminosity: it shows a relatively strong correlation between the PAH 11.3/7.7 ratio and [OIII] luminosity. The correlation coefficient is $\tau = -0.5099$.

Table 3 Correlation of Eigenvectors with Line and Continuum Properties

Property	Eigenvector 1 40.7326%	Eigenvector 2 60.7867%	Eigenvector 3 77.3882%	Eigenvector 4 87.7519%	Eigenvector 5 94.5503%
PAH 11.3 μm EW	0.5479	0.2541	0.2503	0.7520	0.0838
L(PAH 11.3 μm)	0.4282	0.7458	−0.4273	−0.1008	−0.0362
PAH 11.3 μm/7.7 μm	0.8561	0.1651	−0.1274	−0.2247	0.2949
RFe	0.7426	0.3195	0.3648	−0.2215	−0.3074
L[OIII]	−0.7142	0.5439	0.0361	0.0784	−0.3455
Hβ asymm	0.7071	−0.5251	0.1984	−0.0177	−0.3397
$\log R$	0.2703	−0.2863	−0.8526	0.2093	−0.2265

where $D_{\rm L}$ (luminosity distance) is calculated by Wright's Javascript Cosmology Calculator tool on the NED webpage, with a cosmology of $H_0 = 71\ {\rm km\ s^{-1}\ Mpc^{-1}}$, $\Omega_M = 0.27$ and $\Omega_{\rm vac} = 0.73$.

The results of the principal component analysis are listed in Table 3. We chose to perform the principal component analysis on seven parameters. They are PAH EW 11.3 μm, PAH 11.3 μm luminosity, PAH 11.3/7.7 ratio, RFe, [OIII] luminosity, Hβ asymmetry and $\log R$ (the ratio of radio-to-

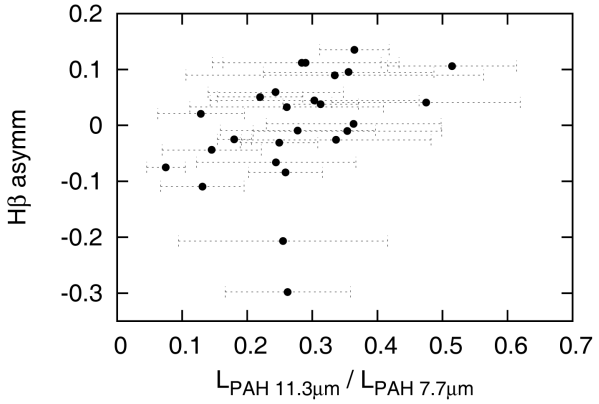

Fig. 5 PAH 11.3 μm/PAH 7.7 μm vs. Hβ asymmetry: it shows a correlation between the PAH 11.3/7.7 ratio and Hβ asymmetry. The correlation coefficient is $\tau = 0.3989$.

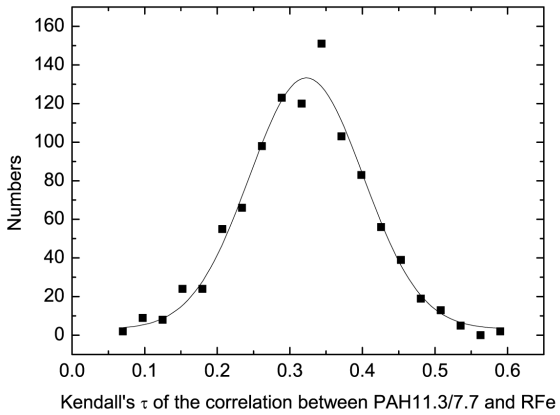

Fig. 6 Kendall's τ vs. numbers: distribution of the simulated Kendall's τ for the PAH ratio vs. RFe correlation. The best fit Gaussian function is shown by the solid line.

optical luminosity), each of which contains potentially unique information. The first five significant eigenvectors are listed in Table 3. Our PCA analysis confirms that the PAH 11.3/7.7 ratio is strongly related with E1.

In order to investigate the effect of errors on these correlations, we performed Monte Carlo simulations, with each one having 1000 random experiments. The random numbers that represent EWs of PAHs were generated by assuming a constant distribution within an error of 0.005. The random numbers corresponding to the PAH 11.3/7.7 ratio were produced by a Gaussian distribution under certain constraints for the errors. Then Kendall's τ test was applied to each random sample.

Figure 6 shows the distribution of the simulated Kendall's τ for the correlation between the PAH ratio and the RFe as an example of the Monte Carlo tests. The distribution can be described by a Gaussian function with a peak at $\tau = 0.343$ and standard deviation $\sigma = 0.076$. The percentage of all the Monte Carlo tests with $p \leq 0.05$ (indicating there is a statistically significant correlation) is 90.3%. All the results of the Monte Carlo simulations are listed in Table 4.

Table 4 The Results of Monte Carlo Simulations

	Peak of τ	σ	Percentage of tests with $p \leq 0.05$
PAH 11.3 μm EW vs. RFe	0.218	0.019	50.9%
PAH 11.3 μm/7.7 μm vs. RFe	0.343	0.076	90.3%
PAH 11.3 μm/7.7 μm vs. OIII luminosity	–0.355	0.075	87.4%
PAH 11.3 μm/7.7 μm vs. Hβ asymm	0.323	0.079	68.2%

4 DISCUSSION

Fortunately, 42 out of 47 AGNs (89% of our sample) come from Shi et al. (2007), of which 40 AGNs are PG quasars from BG92. Kendall Rank-Order tests are performed on this sub-sample. Tests return $\tau = 0.4215$ and $p = 0.0025$ for the PAH 11.3/7.7 ratio versus RFe with 26 AGNs, $\tau = -0.4373$ and $p = 0.0044$ for the PAH 11.3/7.7 ratio versus [OIII] luminosity with 22 AGNs, and $\tau = 0.3662$ and $p = 0.0087$ for the PAH 11.3/7.7 ratio versus Hβ asymmetry with 26 AGNs. These correlation coefficients are similar to those of the whole sample. On the other hand, Eigenvector 1 and Eigenvector 2 of our sample are consistent with those of BG92. E1 is dominated by RFe, [OIII] luminosity and Hβ asymmetry. Our sample indicates that the PAH 11.3/7.7 ratio is obviously related to E1.

The PAH 11.3 μm feature is thought to be emitted by a neutral grain and the 7.7 μm feature by an ion. According to Draine & Li (2001), the PAH 11.3/7.7 ratio is mainly driven by ionization and increases with the amount of neutral PAHs. The strong correlation between the PAH 11.3/7.7 ratio and E1 indicates that AGNs with high RFe, weak [OIII] emission and a strong Hβ blue-wing are likely to have low PAH ionization and hence a larger amount of neutral PAHs.

LaMassa et al. (2012) selected a Type-II AGN sample from the Sloan Digital Sky Survey. The PAH 11.3/7.7 ratios of their sample were obtained from *Spitzer* IRS, and range from 0.15 to 0.45, which is quite similar to our sample. A significant correlation between the PAH 7.7/11.3 ratio and the optical D parameter was found in their sample. The optical D parameter is the distance a source lies on the BPT diagram (used for identifying AGNs) from star-forming galaxies (Kauffmann et al. 2003), so that a larger D statistically indicates a greater dominance of AGN activity and corresponds to an older stellar population (Kewley et al. 2006). LaMassa et al. (2012) also noticed that there is a significant correlation between the PAH 7.7/11.3 ratio and [Ne V]/[Ne II]. The [Ne V] line is only detected in optically classified AGNs (with few exceptions). Thus, [Ne V]/[Ne II] is an indicator of radiation hardness, and is also a diagnostic of the relative importance of AGN activity (Armus et al. 2007; Veilleux et al. 2009; Pereira-Santaella et al. 2010). A greater dominance of AGN activity, older stellar populations and harder radiation correspond to a smaller PAH 11.3/7.7 ratio.

In this paper, we found that the PAH 11.3/7.7 ratio has an obvious correlation with E1. AGNs with smaller RFe, stronger [OIII] luminosity and a red Hβ wing correspond to a lower PAH 11.3/7.7 ratio. Boroson (2002) concluded that E1 is dominantly driven by the Eddington ratio and AGNs with a lower Eddington ratio tend to have smaller RFe. Based on an IRAS 25 μm and 60 μm selected type-I AGN sample, Wang et al. (2006) pointed out that E1 is related to the nuclear star-formation history. AGNs with an older stellar population have a statistically smaller RFe. The correlation between the Eddington ratio and the age of a stellar population has been confirmed by Wang & Wei (2008) in an optically selected Type-I AGN sample, and by Wang et al. (2013) in an X-ray selected Type-II AGN sample. AGNs with an older stellar population in the host galaxy have statistically harder 2–10 keV X-ray emission and a lower Eddington ratio (Wang et al. 2013). Therefore, the behavior of the PAH 11.3/7.7 ratio recovered in Type-I AGNs by this paper is consistent with what has been found in Type-II AGNs by LaMassa et al. (2012).

5 CONCLUSIONS

In order to explore the relationship between properties of PAHs and AGN activities, we selected a sample of 47 Type-I AGNs with *Spitzer* IRS data from the literature. It is found that the PAH 11.3/7.7 ratio has a correlation with RFe, [OIII]λ5007 luminosity and Hβ asymmetry. Results of principal component analysis revealed that the PAH 11.3/7.7 ratio is correlated with the primary elements in E1 of Type-I AGNs. The obvious correlation between the PAH 11.3/7.7 ratio and E1 indicated that AGNs with high RFe, weak [OIII] emission and strong blue-wing Hβ are likely to have a low PAH ionization and more neutral PAHs. We also noticed that our results are consistent with the results of LaMassa et al. (2012) from the Type-II AGN sample.

Acknowledgements We would like to thank the anonymous referee for their helpful suggestions. We are very grateful for help from Aigen Li. We also want to thank Xianmeng Meng, Hao Liu, Hongbo Cai and Yuanfeng Xuan for their help. This work was supported by the National Basic Research Program of China (973 program, 2014CB845800) and the National Natural Science Foundation of China (Grant Nos. 11473036 and U1331202). The work is based in part on observations made with the *Spitzer Space Telescope*, and made use of the NASA/IPAC Extragalactic Database (NED), which is operated by the Jet Propulsion Laboratory, California Institute of Technology, under contract with the National Aeronautics and Space Administration.

References

Allamandola, L. J., Hudgins, D. M., & Sandford, S. A. 1999, ApJ, 511, L115
Allamandola, L. J., Tielens, A. G. G. M., & Barker, J. R. 1985, ApJ, 290, L25
Alonso-Herrero, A., Ward, M. J., & Kotilainen, J. K. 1997, MNRAS, 288, 977
Armus, L., Charmandaris, V., Bernard-Salas, J., et al. 2007, ApJ, 656, 148
Bonatto, C. J., & Pastoriza, M. G. 1997, ApJ, 486, 132
Boroson, T. A. 2002, ApJ, 565, 78
Boroson, T. A., & Green, R. F. 1992, ApJS, 80, 109 (BG92)
Brightman, M., & Nandra, K. 2011, MNRAS, 414, 3084
Buchanan, C. L., Gallimore, J. F., O'Dea, C. P., et al. 2006, AJ, 132, 401
Clavel, J., Schulz, B., Altieri, B., et al. 2000, A&A, 357, 839
De Robertis, M. 1985, ApJ, 289, 67
Diamond-Stanic, A. M., & Rieke, G. H. 2010, ApJ, 724, 140
Draine, B. T., & Lee, H. M. 1984, ApJ, 285, 89
Draine, B. T., & Li, A. 2001, ApJ, 551, 807
Galliano, F., Madden, S. C., Tielens, A. G. G. M., Peeters, E., & Jones, A. P. 2008, ApJ, 679, 310
Genzel, R., & Cesarsky, C. J. 2000, ARA&A, 38, 761
Grupe, D. 2004, AJ, 127, 1799
Grupe, D., Beuermann, K., Mannheim, K., & Thomas, H.-C. 1999, A&A, 350, 805
Grupe, D., Wills, B. J., Leighly, K. M., et al. 2004, AJ, 127, 156
Higdon, S. J. U., Devost, D., Higdon, J. L., et al. 2004, PASP, 116, 975
Kauffmann, G., Heckman, T. M., & Tremonti, C., et al. 2003, MNRAS, 346, 1055
Kewley, L. J., Groves, B., Kauffmann, G., & Heckman, T. 2006, MNRAS, 372, 961
Kraemer, S. B., George, I. M., Crenshaw, D. M., & Gabel, J. R. 2004, ApJ, 607, 794
Kuraszkiewicz, J., Wilkes, B. J., Brandt, W. N., & Vestergaard, M. 2000, ApJ, 542, 631
LaMassa, S. M., Heckman, T. M., Ptak, A., et al. 2012, ApJ, 758, 1
Laor, A., Fiore, F., Elvis, M., Wilkes, B. J., & McDowell, J. C. 1997, ApJ, 477, 93
Lawrence, A., Elvis, M., Wilkes, B. J., McHardy, I., & Brandt, N. 1997, MNRAS, 285, 879
Leger, A., & Puget, J. L. 1984, A&A, 137, L5

Maiolino, R., Shemmer, O., Imanishi, M., et al. 2007, A&A, 468, 979
Mao, Y.-F., Wang, J., & Wei, J.-Y. 2009, RAA (Research in Astronomy and Astrophysics), 9, 529
Meléndez, M., Kraemer, S. B., Armentrout, B. K., et al. 2008, ApJ, 682, 94
Ogle, P., Boulanger, F., Guillard, P., et al. 2010, ApJ, 724, 1193
Peeters, E., Spoon, H. W. W., & Tielens, A. G. G. M. 2004, ApJ, 613, 986
Pereira-Santaella, M., Alonso-Herrero, A., Rieke, G. H., et al. 2010, ApJS, 188, 447
Puget, J. L., & Leger, A. 1989, ARA&A, 27, 161
Shi, Y., Ogle, P., Rieke, G. H., et al. 2007, ApJ, 669, 841
Smith, J. D. T., Armus, L., Dale, D. A., et al. 2007a, PASP, 119, 1133
Smith, J. D. T., Draine, B. T., Dale, D. A., et al. 2007b, ApJ, 656, 770
Stockton, A., & MacKenty, J. W. 1987, ApJ, 316, 584
Sulentic, J. W., Marziani, P., & Dultzin-Hacyan, D. 2000, ARA&A, 38, 521
Sulentic, J. W., Marziani, P., Zamanov, R., et al. 2002, ApJ, 566, L71
Sulentic, J. W., Stirpe, G. M., Marziani, P., et al. 2004, A&A, 423, 121
Tommasin, S., Spinoglio, L., Malkan, M. A., et al. 2008, ApJ, 676, 836
van der Wolk, G., Barthel, P. D., Peletier, R. F., & Pel, J. W. 2010, A&A, 511, AA64
Vaughan, S., Edelson, R., Warwick, R. S., Malkan, M. A., & Goad, M. R. 2001, MNRAS, 327, 673
Veilleux, S., Rupke, D. S. N., Kim, D. -C., et al. 2009, ApJS, 182, 628
Wang, T., Brinkmann, W., & Bergeron, J. 1996, A&A, 309, 81
Wang, J., Wei, J. Y., & He, X. T. 2006, ApJ, 638, 106
Wang, J., & Wei, J. Y. 2008, ApJ, 679, 86
Wang, J., Zhou, X. L., & Wei, J. Y. 2013, ApJ, 768, 176
Whittle, M. 1992, ApJS, 79, 49
Xu, D. W., Komossa, S., Wei, J. Y., Qian, Y., & Zheng, X. Z. 2003, ApJ, 590, 73
Zhang, E.-P., & Wang, J.-M. 2006, ApJ, 653, 137